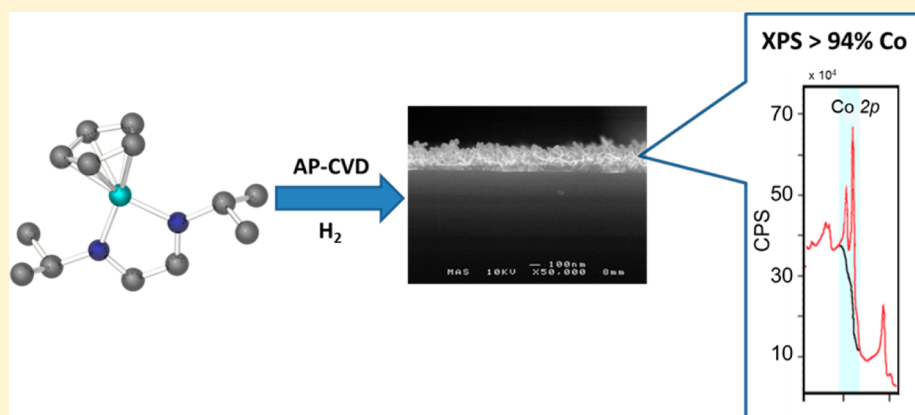# Cobalt(III) Diazabutadiene Precursors for Metal Deposition: Nanoparticle and Thin Film Growth

Thomas Pugh,[†] Samuel D. Cosham,[†] Jeff A. Hamilton,[†] Andrew J. Kingsley,[‡] and Andrew L. Johnson*,[†]

[†]Department of Chemistry, University of Bath, Bath, BA2 7AY, United Kingdom
[‡]SAFC-Hitech, Power Road, Bromborough, Wirral, CH62 3QF, United Kingdom

Ⓢ *Supporting Information*

ABSTRACT: We report the synthesis and characterization of a family of cobalt(III) metal precursors, based around cyclopentadienyl and diazabutadiene ligands. The molecular structure of the complexes cyclopentadienyl-Cobalt(III)(*N*,*N'*-dicyclohexyl-diazabutadiene) (**2c**) and cyclopentadienyl-Cobalt(III)(*N*,*N'*-dimesityl-diazabutadiene) (**2d**) are described, as determined by single crystal X-ray diffraction analysis. Thermogravimetric analysis of the complexes highlighted the isopropyl derivative CpCo(^{i}Pr$_2$-dab) (**2a**) as a possible cobalt metal chemical vapor deposition (CVD) precursor. Atmospheric pressure CVD (AP-CVD) was employed using precursor **2a** to synthesize thin films of metallic cobalt on silicon substrates under an atmosphere of hydrogen (H$_2$). Analysis of the thin films deposited at substrate temperatures of 250 °C, 275 °C, 300 °C, 325 °C, and 350 °C, respectively, by scanning electron microscopy (SEM) and atomic force microscopy (AFM) reveal temperature dependent growth features: films grown at 325 and 350 °C are continuous and pinhole free, whereas those films grown at substrate temperatures of 250 °C, 275 °C, and 300 °C consist of crystalline nanoparticles. Powder X-ray diffraction (PXRD) and X-ray photoelectron spectroscopy (XPS) all show the films to be high purity metallic cobalt. Raman spectroscopy has also been used to prove the absence of cobalt silicides at the substrate/thin film interface.

■ INTRODUCTION

Metal thin films and nanostructures are in demand for a range of technological applications, finding use as active materials in microelectronics, sensors, and catalysts, as well as reflective and refractive coatings for optical devices, and as decorative and/or protective coatings.[1] Thin films of cobalt, cobalt oxide, cobalt alloys, and cobalt/X multilayers (where X is a nonmagnetic or insulating material) have all been the subject of renewed interest over the past decade because of their relevance to magnetic devices utilizing phenomena such as giant magneto-resistance (GMR)[2] and tunneling magnetoresistance (TMR),[3] since cobalt exhibits the highest magnetic anisotropy of any transition metal.[4] A major motivation for cobalt film growth has been the formation of CoSi$_2$,[5] which can act as both metallic interconnections and ohmic contacts in silicon based devices, as well as Schottky contacts in the field of optoelectronics,[6] and as metal caps for copper interconnects.[7] More recently, cobalt and

especially porous cobalt films have been found to be active materials for the evolution of oxygen and hydrogen in alkaline solutions.[8] Thin films of cobalt and cobalt oxide have also found utility as components of energy storage devices, for example, LiCoO$_2$ in lithium ion batteries.[9] Resultantly cobalt thin films have been deposited by various means including electrodeposition,[10] sputtering,[11] electron beam evaporation,[12] chemical vapor deposition (CVD),[6c,13] and more recently atomic layer deposition (ALD).

Research has demonstrated that CVD is capable of depositing thin cobalt films of higher quality than sputtering methods. However, despite the advantages of increased thin film purity and uniformity there are limited reports of cobalt CVD, and more specifically, the development of novel chemical

Chart 1. Co Metal CVD and ALD Precursors Reported in the Scientific Literature to-Date

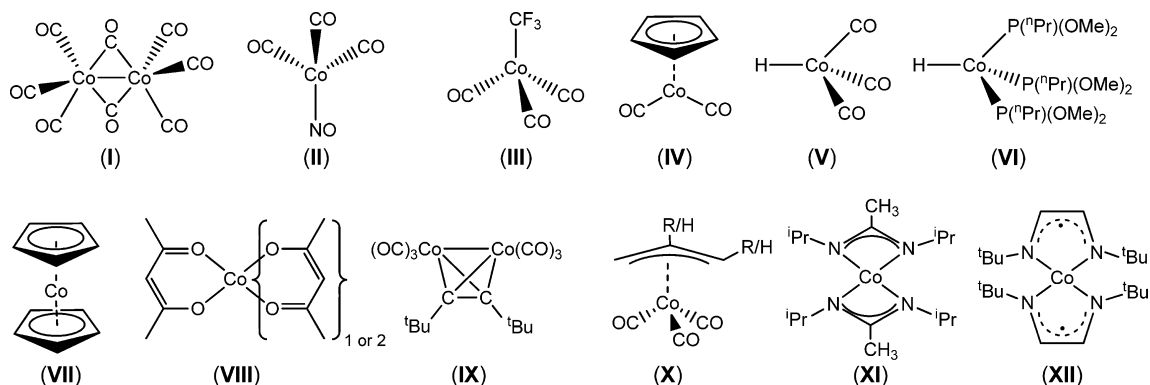**Table 1. Diazabutadiene Ligands Used in This Study**

	R
1a	*iso*-Propyl
1b	*tert*-Butyl
1c	Cyclohexyl
1d	2,4,6-Trimethylphenyl
1e	2,6-Diisopropylphenyl

precursors. To date, the literature has only highlighted a limited number of cobalt CVD precursors which include $Co_2(CO)_8$ (**I**),[6e,11c,13d,k,m] $Co(NO)(CO)_3$ (**II**),[6a,13e,k,14] $CoCF_3(CO)_4$ (**III**),[13d] $CpCo(CO)_2$ (**IV**),[6d–h,13c,d] $CoH(CO)_4$ (**V**),[15] CoH-$[^nPrOP(OMe)_2]_3$ (**VI**),[16] Cp_2Co (**VII**),[13d] $Co(acac)_{2/3}$ (**VIII**),[13i,l,17] $Co_2(CO)_6(\mu^2-C_2(H)^tBu)$ (**IX**),[13h] and $Co(Allyl)$-$(CO)_3$ (**X**)[18] (Chart 1).

The paucity of chemical literature concerning the production of cobalt thin films is largely due to the limited number of precursors displaying both volatility and thermal stability. For example, as solids at operation temperature, $Co_2(CO)_8$ (**I**), Cp_2Co (**VII**), and $Co(acac)_2$ (**VIII**) all suffer from variable vapor pressures, caused by changing precursor surface area during processing, which results in unreliable thickness control and the possibility of film contamination from the shedding of particles.[13d,l] In contrast $Co(CO)_3(NO)$ (**II**), which is a liquid with a high vapor pressure, is susceptible to the incorporation of carbon, oxygen, and nitrogen impurities associated with ligand decomposition, requiring exceedingly stringent conditions to avoid contamination of the thin films deposited.[6a,13e,k,14]

The liquid precursor material $CpCo(CO)_2$ (**IV**) is a volatile (0.5 Torr at 25 °C) precursor which has been widely investigated as a CVD precursor to both cobalt metal and cobalt silicide. While the literature has shown atmospheric pressure-CVD (AP-CVD) of (**IV**) in a H_2 atmosphere to yield high purity cobalt films (99%) at rates of up to 60 Å/min, low pressure-CVD (LP-CVD) of (**IV**) invariably leads to films heavily contaminated with carbon.[13c] In addition, the precursor needs to be stored at low temperatures to prevent decomposition during storage, a problem common to the entire range of carbon monoxide containing precursors (**I**–**V**, **IX**, and **X**).

While recent focus has been directed toward lower temperature growth methods, such as ALD and plasma assisted-ALD, to avoid dewetting and nanoparticle growth,

precursor development has not advanced at an equal pace, with precursors such as $Co_2(CO)_8$ (**I**),[19] $CpCo(CO)_2$ (**IV**),[20] Cp_2Co (**VII**),[20,21] and $Co(Allyl)(CO)_3$ (**X**),[22] originally developed for CVD, featuring as precursors for ALD of cobalt metal. Only very recently has there been resurgence in the development of new cobalt metal precursors, with the publication of the synthesis of stable and highly volatile complexes of cobalt such as the *bis*-amidinate complex (**XI**)[20,23] and *bis*-diazadienyl (**XII**)[24] complexes alongside their application in the ALD of thin films of cobalt metal and cobalt oxide.[25]

The general lack of suitable precursors for cobalt deposition highlights a need for the design and development of novel precursors which amalgamate desirable properties such as thermal stability and high volatility and are capable of depositing highly pure films at low deposition temperatures. Herein, we report the synthesis, thermogravimetric analysis (TGA), and AP-CVD of a series of organometallic Co(III) precursors containing N,N'-dialkyldiazabutadiene and N,N'-diaryldiazabutadiene, $(R_2$-dab) ligands **1a**–**e**, (Table 1) of the general form $(\eta^5-C_5H_5)Co(R_2$-dab). It should be made clear here, that several of the complexes reported ibid. (**2a**, **2b** and **2e**) have been synthesized previously by Dieck et al. using alternative routes,[26] but these complexes have never before been investigated for their volatility and potential utility in the deposition of cobalt metal thin films, while molecular structures of the complexes **2c** and **2d** are reported here for the first time.

Diazabutadiene (or α-diimine) ligands have attracted significant interest because of their ability to stabilize metal centers in formally low oxidation states, a direct consequence of the presence of a low lying ligand-based π^* orbital, capable of accepting electron density from the metal containing fragment.[26] This orbital can also be occupied through metal-to-ligand charge transfer (MLCT), through facile, and reversible, chemical or electrochemical reduction or through direct ground state metal-to-ligand two-electron transfer. As a consequence of their noninnocent redox behavior these ligands, when attached

to a metal center have been shown to exist in one of four distinct forms each with distinguishing structural features (Chart 2): (i) a dative coordination of the nitrogen atoms to

**Chart 2. Possible Forms of the Metal Diazabutadiene Systems**

the metal atom (form **A**) with short carbon−nitrogen bonds, long carbon−carbon and metal−nitrogen bonds, (ii) a dative coordination of the nitrogen atoms to the metal atom with associated back bonding from the metal into the π^* orbital of the ligand (form **B**) with intermediate carbon−carbon and carbon−nitrogen bonds and short metal−nitrogen bonds, (iii) a single electron reduced delocalized diazabutadiene anion coordination to the metal, with intermediate carbon−carbon and carbon−nitrogen bonds and long metal−nitrogen bonds (form **C**), and (iv) a two-electron reduced diamide ligand, with short metal−nitrogen and carbon−carbon bonds and long carbon−nitrogen bonds (**D**).

While an examination of the literature shows that the η^2-R$_2$-dab coordination mode is the most prevalent,[27] R$_2$-dab ligands can also bind to metal centers in an η^4-{N$_2$C$_2$} coordination mode to form π-complexes with metals.[28]

■ RESULTS AND DISCUSSION

Synthesis. Complexes **2a−e** were prepared by the reaction of ClCo(PPh$_3$)$_3$ with NaCp, followed by a thermally driven substitution of PPh$_3$ with the appropriate N,N'-dialkyldiazabutadiene (Scheme 1). Complex **2a** was isolated as a dark brown

Scheme 1. Outline of the Synthetic Methodology Used in the Production of Complexes 2a−e
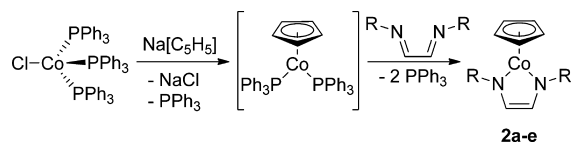
oil and purified by distillation (5 × 10^{-2} mbar, 100 °C), complexes **2b** and **2c** were isolated as dark brown solids purified by sublimation (5 × 10^{-2} mbar, 100 °C) and complexes **2d** and **2e** were isolated by recrystallization from saturated hexane solutions at −28 °C.

Room temperature ^{1}H NMR of complexes **2a−e** showed all of the complexes to be diamagnetic,[26] and to possess characteristic singlet resonances for η^5-Cp-$\underline{H}$ between δ = 4.1 and 4.8 ppm; R$_2$-dab backbone protons (C$\underline{H}$) showed singlet resonances in the range of δ = 6.6−7.2 ppm. ^{1}H NMR resonances for the alkyl and aryl substituents attached to the coordinated R$_2$-dab ligands were also present. Upon coordination of the R$_2$-dab ligands to the cobalt atom there is a notable change in the chemical shift for both C$\underline{H}$ groups, and N-alkyl or N-aryl substituents, for example, N,N'-di-isopropyl-diazabutadiene backbone C$\underline{H}$-resonances for uncoordinated (**1a**) and coordinated (**2a**) are δ = 7.9 ppm and 7.0 ppm respectively; correspondingly the methine C$\underline{H}$ of the isopropyl substituent changes from δ = 3.5 ppm to δ = 4.9 ppm upon coordination to the cobalt.

Molecular Structures of 2c and 2d. Of the five complexes reported in this study, single crystals suitable for single crystal X-ray diffraction of only two complexes, **2c** and **2d**, could be isolated; these were grown from saturated hexane solutions at −28 °C and were structurally characterized by single crystal X-ray diffraction to unambiguously determine the solid state molecular structures of the products. Experimental crystallographic data are summarized in Table 2, selected bond lengths and angles for **2c** and **2d** are shown in Table 3, and the molecular structures of the complexes are shown in Figure 1.

Table 2. Crystallographic Data for the Complexes 2c, and 2d

	2c	2d
empirical formula	C$_{19}$H$_{29}$CoN$_2$	C$_{25}$H$_{29}$CoN$_2$
formula weight	344.37	416.43
T/K	150(2)	150(2)
crystal system	triclinic	monoclinic
space group	$P\bar{1}$	$P2_1/a$
a (Å)	8.4720(10)	7.8580(4)
b (Å)	10.4340(10)	31.7460(18)
c (Å)	10.952(2)	9.0620(4)
α (deg)	105.676(4)	
β (deg)	107.831(4)	112.482(3)
γ (deg)	96.116(9)	
V	868.2(2)	2088.80(18)
Z	2	4
ρ_{calc} mg/m^{-3}	1.317	1.324
μ(Mo−K$_\alpha$), mm^{-1}	0.987	0.834
$F(000)$	1.040	880
crystal size, mm	0.40 × 0.20 × 0.05	0.20 × 0.17 × 0.05
θ range (deg)	2.68 to 25.00	2.75 to 27.50
reflections collected	14683	19648
independent reflections [R(int)]	3043 [R(int) = 0.0447]	4606 [R(int) = 0.1655]
max.,min transmission	0.8501 and 0.8270	0.9595 and 0.8509
goodness-of-fit	1.040	1.018
final R1 (wR_2) [$I > 2\sigma(I)$]	R_1 = 0.0291, wR_2 = 0.0670	R_1 = 0.0754, wR_2 = 0.0861
final R1 (wR_2) (all data)	R_1 = 0.0333, wR_2 = 0.0693	R_1 = 0.2204, wR_2 = 0.1206
largest diff. peak and hole, e Å^{-3}	0.280 and −0.539	0.454 and −0.535

In the solid state complexes **2c** and **2d** adopt mononuclear structures, in which the metal centers possess a *pseudo*-trigonal planar environment, comparable to the related iridium-dab complex [Cp*Ir(R$_2$dab)] (R = 2,6-dimethylphenyl),[29] the diaryltetraazadiene complexes [CpCo(Ar$^f_2$N$_4$)] (Ar^f = C$_6$F$_5$)

Table 3. Selected Bond Lengths and Angles for 2c and 2d

	2c	2d
	Bond Distances (Å)	
Co-(η^5-C$_5$H$_5$)$_{(cent)}$	1.695	1.677
Co−N(1)/Co−N(2)	1.887(2)/1.859(2)	1.855(4)/ 1.844(6)
N=C	1.336(5)/1.332(5)	1.339(7)/ 1.343(7)
C−C	1.382(3)	1.383(6)
	Bond Angles (deg)	
N(1)−Co−N(2)	82.99(7)	82.91(17)
Co−N(1)=C/Co−N(2)=C	113.45(12)/ 114.78(13)	115.0(3)/ 115.3(3)
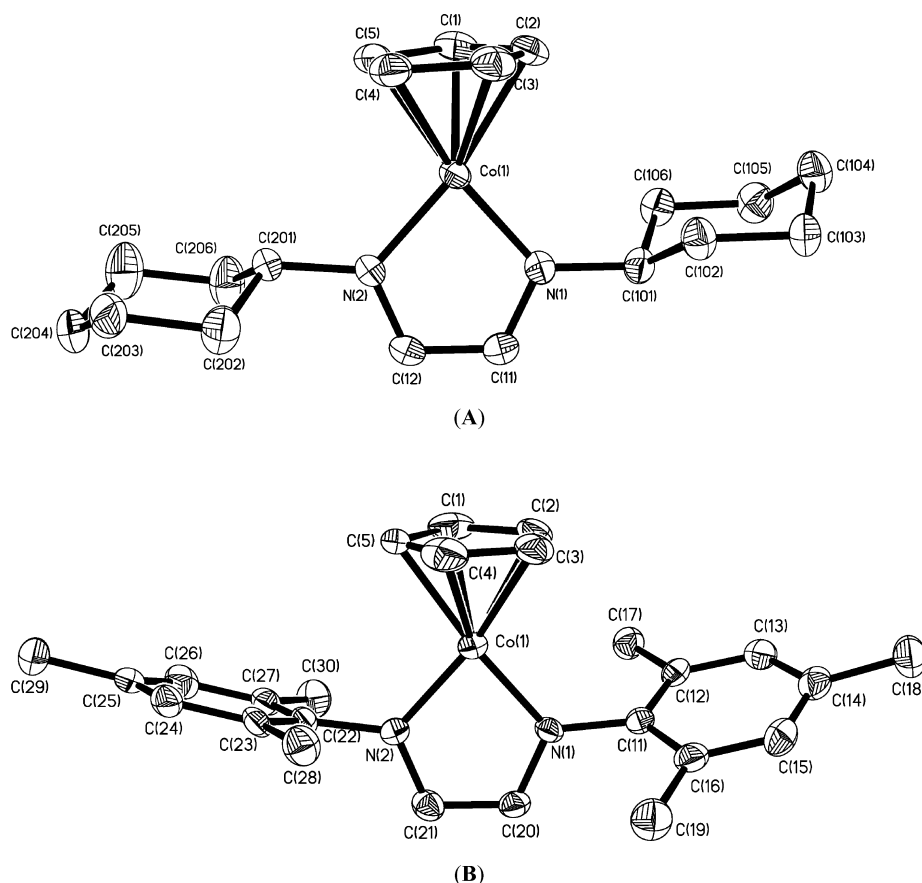
Figure 1. Diagram showing the molecular structures of the complexes **2c** (A) and **2d** (B) (50% probability ellipsoids). Hydrogen atoms have been omitted for clarity.

Table 4. Co−N, N−C, and C−C Bond Distances in Selected Cobalt-dab Complexes

complexes[a]	oxidation state/d^n	Co−N	N−C	C−C	ref
$[(^tBu_2\text{-dab})CoCl_2]$	2+/ d^7	2.07	1.26	1.51	33
$[(Dipp_2\text{-dab})CoBr_2]$	2+/ d^7	2.05	1.34	1.53	34
$[(Ph_2\text{-dab-}Me_2)CoCl_2]$	2+/ d^7	2.04	1.28	1.50	35
$[(Xyl_2\text{-dab-}Me_2)CoBr_2]$	2+/ d^7	2.05	1.28	1.52	36
$[(Mes_2\text{-dab-}Me_2)CoCl_2]$	2+/ d^7	2.05	1.28	1.53	35
$[(Dipp_2\text{-dab-}Me_2)CoCl_2]$	2+/ d^7	2.04	1.29	1.50	35
$[(Dipp_2\text{-dab-}Me_2)CoI_2]$	2+/ d^7	2.05	1.28	1.53	37
$[\{^tBu_2\text{-dab}\}_2Co]$	2+/ d^7	1.93	1.34	1.40	24
$[\{(C_6F_5)_2\text{-dab-}Me_2\}_2Co]$	2+/ d^7	1.93	1.35	1.41	38
$[(^iPr_2\text{-dab})Co(NO)(CO)]$	−1/d^{10}	1.96	1.27	1.44	39
$[(Dipp_2\text{-dab})Co(NO)(CO)]$	−1/d^{10}	1.96	1.30	1.43	39
2c	3+/d^6	1.87	1.34	1.38	this work
2d	3+/d^6	1.85	1.34	1.38	this work
$[Cp^*Ir(Xyl_2\text{-dab})]$	3+/d^6		1.37	1.33	29

[a]Mes =2,4,6-trimethylphenyl; Dipp =2,6-diisopropylphenyl; Xyl =2,6-dimethylphenyl; R_2-dab-Me_2 = R-N=C(Me)-C(Me)=N-R; Cp* = (η^5-C_5Me_5).

and $[CpNi(Ar_2N_4)]$ (Ar = C_6H_4Me)[30] and $[Cp^*Co(Bipy)]$,[31] all of which share a common structural form based on the similarities of the nitrogen containing ligand systems. In both **2c** and **2d** the $\{CoN_2C_2\}$ rings are planar (the mean deviation of an atom in the ring from the least-squares plane of the ring being 0.0007 Å and 0.0051 Å respectively) and the Cp ligands are essentially orthogonal to the $\{CoN_2C_2\}$ plane (**2c**: 89.60°, **2d**: 89.85°).

The average Co−N bond lengths of about 1.870 Å are relatively short compared to other structurally characterized Co-R_2-dab systems and are much more comparable to Co−N single bonds found in cobalt-amide complexes,[32] in which Co−N secondary interactions (multiple bond character) are invoked (cf. Co=N: 1.66−1.68). The precise oxidation state of the ligands, and consequently of the metal centers in dab-complexes have previously been assigned, by others, on the basis of a comparison of the M−N, N−C, and C−C bond lengths within complexes, in which the ligands are either neutral (dab), radical monanions ($[dab]^{•−}$) or dianionic ligands ($[dab]^{2−}$). A comparison of the Co−N, N−C and C−C bond

lengths of the R₂-dab ligands in complexes **2c** and **2d** with related Co-dab containing complexes is shown in Table 4.

A comparison of the bond parameters in Table 4 suggest that the complexes fall into several distinct classes with respect to the oxidation state of the dab ligands, and hence the Co atom. The simple Co dihalide complexes, for example, [(^tBu₂-dab)CoCl₂], display a distribution of bond lengths which have previously been ascribed to α-diimine coordination complexes in which the neutral diimine ligand possess alternating long Co−N; short N−C; long C−C, bonds representative of single/double/single bond character (form **A**, Chart 2). In contrast, the *bis*-dab cobalt complex, [{^tBu₂-dab}₂Co] and [{(C₆F₅)₂-dab-Me₂}₂Co], which have been unequivocally described as Co(II) complexes containing two radical monoanionic [dab]^•− ligands, clearly show a lengthening of the N−C bonds and a concomitant shortening of the Co−N/C−C bonds, indicative of a single electron delocalized about the π-orbitals of the dab ligand (form **C**, Chart 2). Both of these types of system are ascribed a Co(II) oxidation state (d⁷ electronic configuration); an observation that is confirmed by the paramagnetic nature of the complexes and density functional theory (DFT) calculations, and in the case of [{^tBu₂-dab}₂Co] and [{(C₆F₅)₂-dab-Me₂}₂Co] by SQUID measurements and electron spin resonance (ESR) spectroscopy which are consistent with a divalent Co d⁷ ion and a pair of radical monoanionic ligands.

The Co complexes, [(^iPr₂-dab)Co(NO)(CO)] and [(Dipp₂-dab)Co(NO)(CO)], reported by Kaim et al. display, what are ascribed as bond lengths which are intermediate between the α-diimine complexes and the cobalt(II) diimine diradical complexes.[39] These diamagnetic complexes are recognized by Kaim et al. as formally Co(-I) species with nonreduced dab ligands and a d¹⁰-configured metal atom. Bond length distortions away from the long/short/long pattern expected in simple α-diimine complexes is effected by π-back bonding from the metal center into the π* orbital of the diimine ligand (form **B**, Chart 2).

An examination of the Co−N/N−C/C−C bond lengths in complexes **2c** and **2d** suggest a different bonding model to those previously discussed; as noted earlier in comparison to the related systems shown in Table 4 the Co−N bonds in **2c/d** are short, with the C−N/C−C bond lengths in strong agreement with what would be expected for a doubly reduced [dab]²− ligand with single N−C and double C−C bonds (form **D**, Chart 2). Complexes **2c/d** are both unequivocally 18-electron diamagnetic complexes, with computational studies suggesting a closed shell d⁶-electronic configuration and a formal Co(III) oxidation state,[26,29] which is in agreement with the related iridium complex [Cp*Ir(R₂dab)] (R = 2,6-dimethylphenyl).[29]

In the solid state the cyclohexyl substituents in **2c** are both arranged in a chair conformation but with one cyclohexyl group oriented toward the {Cp} ligand and the other directed away from the {Cp} ligand; resultantly the centroid of the {Cp} ligand deviates from the nominal C_2 axis of the complex by 2.94° (Figure 2), presumably to reduce steric strain in the solid state. In comparison **2d**, in which the mesityl substituents (viz. their planes) are oriented roughly orthogonal to {CoN₂C₂} plane [N(1)−C(12)−C(17): 73.56°, N(2)−C(22)−C(27): 82.89°], experience no similar distortion in the solid state.

Thermal Profile of Complexes and Use as Deposition Precursors. Thermogravimetric analyses (TGA) of complexes
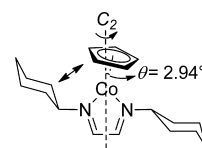
Figure 2. Diagram showing the distortion away from linearity of the Co-Cp_(cent) vector in **2c**.

2a−e were performed to gain insight into relative volatilities and thermal stabilities (Figure 3).
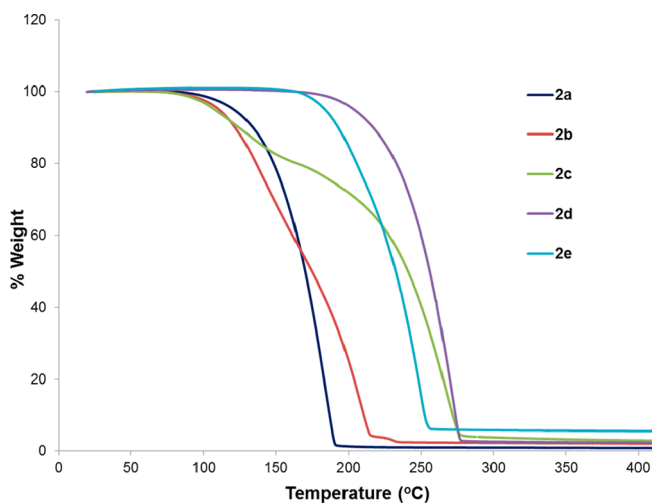
Figure 3. TGA traces of **2a−e** from 30 to 400 °C. Experiments were run under N₂ (50 mL/min) at a ramp rate of 20 °C/min.

These analyses were carried out with an instrument that was housed in a nitrogen filled purge-box to minimize reaction with atmospheric moisture/air. Compounds **2a−e** were found to undergo mass loss to yield stable residues of between 1.5 and 6.3%, over the temperature range 190−280 °C, which are lower than the expected values for cobalt metal from each respective complex (Table 5) indicating a significant degree of

Table 5. Expected % Residue, % of Non-Volatile Residue and Onset Temperature of Volatilization/Decomposition for 2a−e

precursor	expected % for Co	% nonvolatile residue (temp.)	onset temp.[a]
2a	22.3%	1.5% (190 °C)	98 °C
2b	20.2%	4.6% (215 °C)	89 °C
2c	17.1%	4.3% (280 °C)	95 °C
2d	14.2%	3.6% (275 °C)	183 °C
2e	11.8%	6.3% (255 °C)	171 °C

[a]The temperature at which 1% mass loss has occurred.

volatilization in all cases. Complexes **2b** and **2c** appear to have multistep decomposition pathways, as indicated by the changing gradient of the TGA curve, a feature which is much more pronounced for the cyclohexyl-derivative **2c**. In contrast **2a**, **2d**, and **2e** all have TGA curves which present as a relatively sharp single step weight loss that combine a degree of both volatilization and decomposition. Of the complexes investigated complex **2a**, which is a liquid at room temperature, shows the highest degree of volatility losing approximately 98.5% of its

original mass between 98 and 190 °C, suggesting a high degree of thermal stability.

Combined with its liquid nature at room temperature and high degree of volatilization complex **2a** was deemed a suitable candidate for assessment as a Co deposition precursor.

Cobalt Deposition and Thin Film Analysis. Cobalt was deposited onto silicon (400) wafers using the complex **2a** at atmospheric pressure with a cold-walled Electrogas CVD apparatus. The deposition of cobalt metal was investigated at five different substrate temperatures; 250 °C, 275 °C, 300 °C, 325 °C, and 350 °C, respectively. In all of the deposition runs the precursor and the carrier gas lines were externally heated to 130 °C, and the pressure during deposition was maintained at 760 Torr. H_2 gas was used as the carrier gas at a flow rate of 0.3 L min^{-1}. Table 6 shows the general physical parameters used throughout the deposition experiments.

Table 6. General Physical Parameters for the Atmospheric Pressure CVD (AP-CVD) of Complex 2a

| CVD parameters					
substrate temperature (°C)	250	275	300	325	350
operating pressure (Torr)	760	760	760	760	760
carrier gas	H_2	H_2	H_2	H_2	H_2
carrier flow rate (L min^{-1})	0.7	0.7	0.7	0.7	0.7
bubbler flow rate (L min^{-1})	0.3	0.3	0.3	0.3	0.3
temp of Co-precursor bubbler and carrier gas lines (°C)	130	130	130	130	130
deposition duration (mins)	30	30	30	30	30

Films deposited at temperatures of 300 °C and below appeared powdery, silvery-blue in color and discontinuous to the naked eye, whereas films deposited at 325 and 350 °C appeared metallic and continuous, with some brown discoloration in the latter; scanning electron microscopy (SEM) micrographs of the deposited films are shown in Figures 4 and 5. SEM analysis showed films deposited at a substrate temperature of 300 °C and below to be discontinuous and consist of aggregations of nanoparticulate material, suggesting that initial nucleation on silicon is followed by preferential growth on cobalt.[40] Comparing films deposited at substrate temperatures of 250 and 300 °C, which have similar nucleation

densities, the average size of the aggregates is larger in the latter (154 nm vs 238 nm), which is likely to be a result of faster growth rates at higher deposition temperatures. The nucleation density of films grown at 275 °C was found to be lower, but the aggregate sizes of the nanoclusters are larger (375 nm).

The nanoparticles grown from complex **2a** at temperatures of 300 °C and below exhibit a surprising size regularity within each sample (see Figure 4). More significantly, particle size appears to be related to the deposition temperature, and further studies on controlling the size of cobalt nanoparticles are currently underway.

Films grown at substrate temperatures of 325 and 350 °C are seen to be continuous by SEM indicating rapid nucleation and thin film growth (Figure 5) on silicon. Films grown at 325 °C consist of larger particles, which display excellent surface coverage, whereas films grown at 350 °C consist of cylindrical nanorods which protrude from the surface of the substrate. Cross-sectional SEM imaging (Figure 5) show both films to be continuous, and have excellent thickness uniformity; the thicknesses of films grown at 325 and 350 °C were measured to be 112 and 254 nm, translating to a growth rate of 3.73 nm/min and 8.47 nm/min, respectively, which compares favorably to previously reported cobalt metal deposition precursors. Analysis of the films by atomic force microscopy (AFM) (Figure 6) reveals that films deposited at higher temperatures (350 °C) to be rougher than those grown at 325 °C (Rms = 98 nm (325 °C) and 0.13 μm (350 °C)).

To ascertain the elemental composition of the thin films, analysis by high resolution X-ray photoelectron spectroscopy (XPS) was performed; however, XPS data for films deposited from complex **2a** at 300 °C are not reported because of the inability to obtain reliable measurements as a consequence of the significantly reduced surface coverage and larger particle size. In general, analysis of the as-deposited films revealed the presence of significant peaks associated with carbon (1s = 284 eV) and oxygen (1s = 532 eV). Following an argon etch, peaks associated with metallic cobalt (2s = 926 eV, 2p$_{3/2}$ = 779 eV, LMM = 716 eV, 3s = 101 eV and 3p = 60 eV) increased in intensity and peaks associated with carbon and oxygen reduced significantly. Figure 7 shows a typical example of a cobalt XPS spectrum (deposited at 350 °C) showing the presence of photoelectron peaks associated with metallic cobalt [Co2p
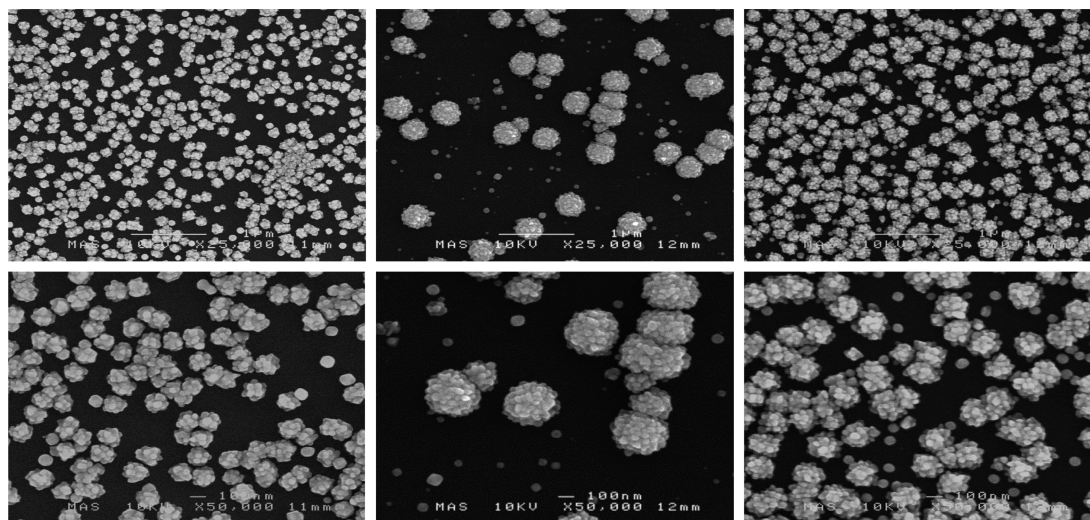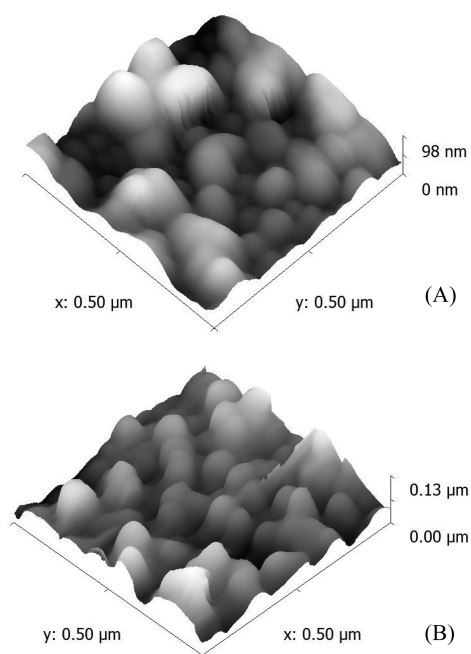

Figure 4. SEM micrographs for films deposited onto Si at 250 °C (left), 275 °C (middle), and 300 °C (right) using complex **2a**.
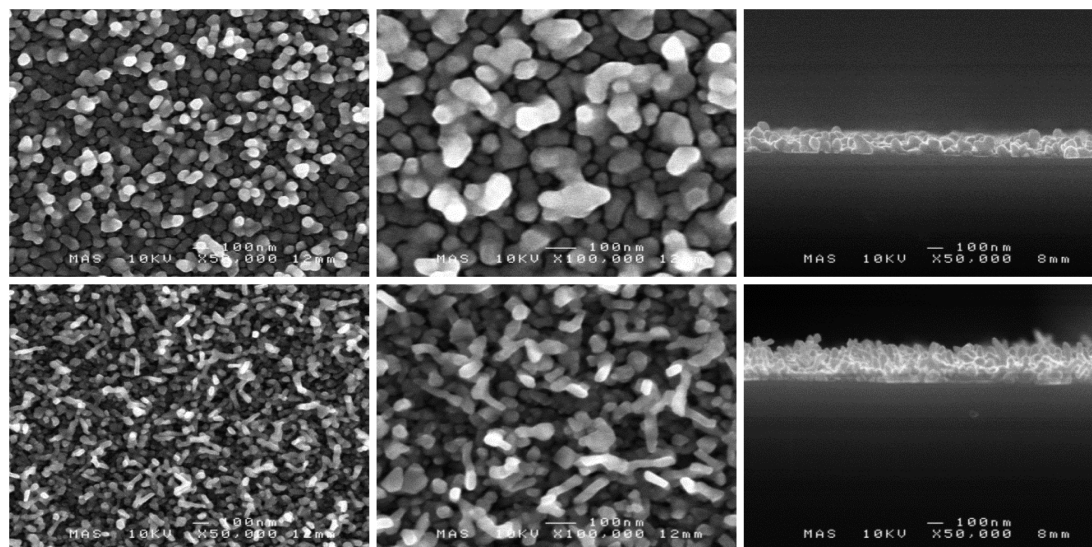
Figure 5. SEM micrographs of films deposited onto Si at 325 °C (top) and 350 °C (bottom) using complex **2a**.

Figure 6. AFM images of the thin film deposited at 325 °C (A) and 350 °C (B) respectively.

region: 793.24 eV (Co 2p$_{1/2}$); 778.04 eV (Co 2p$_{3/2}$)] and the 1s regions for carbon and oxygen, which are common contaminants in deposited cobalt films.

Analysis indicates that films deposited at a substrate temperatures between 250 and 300 °C show a relatively high silicon content; not inconsistent with deposition onto silicon and formation of nanoparticles. In fact in all cases, discounting background silicon values from our calculations suggests that moderately high purity thin films of cobalt have been formed (94.3%, 87.9%, 93.2%, and 90.3% at.% of Co respectively), with unquantifiable traces of carbon and trace amounts of oxygen (Table 7). As the substrate temperature increases to 325 and 350 °C the degree of oxygen contamination increases to 6.17 at.% and 7.52 at.%, respectively, however, carbon contamination remains at low levels. Because of the absence of oxygen within the precursor, oxygen contamination is thought to be a

consequence of ex-situ oxidation of the deposited cobalt films, with the more porous nature of films deposited at 350 °C leading to greater penetration of oxygen and an increase in oxidation. Similarly carbon content in the films is attributed to contamination by atmospheric carbon containing materials post-deposition which can be embedded into films following argon etching.

It is worth noting however, previous reports of cobalt deposition onto silicon substrates, using MOCVD precursors, have been accompanied by the concomitant formation of cobalt silicide materials (i.e., Co$_2$Si, CoSi, and CoSi$_2$),[13e,k,41] although it should also be noted that Co-silicide production is typically a two stage process which involves the deposition of pure Co on Si, typically by physical vapor deposition (PVD) means. This step is followed, in a second stage, by a thermally driven solid state reaction with the Si substrate to grow CoSi$_2$ (>500 °C).[6a,42] In the case of films deposited between 250 to 350 °C there is no evidence from XPS analysis of the formation of Co$_2$Si, CoSi, or CoSi$_2$, all of which are readily identifiable.[42d]

Raman spectroscopy, a technique which is sensitive to the presence of both CoSi and Co$_2$Si, but not CoSi$_2$ and Co phases, was used to further interrogate the nature of the thin-films. While an intense Raman band at 520.9 cm^{-1} revealed the presence of the underlying silicon substrate, no Raman bands attributable to CoSi or Co$_2$Si were observed.[43]

Powder X-ray diffraction (PXRD) analysis (Figure 8) revealed crystal growth in all films deposited using **2a** to be highly selective, showing one intense reflection at $2\theta = 44.3°$ (highlighted in blue, Figure 8), which corresponds to the (111) Miller plane associated with face centered cubic (fcc) cobalt metal;[44] all other reflections are associated with the (400) silicon substrate. Increasing the substrate temperature results in an intensification of the (111) reflection, which is associated with an increasing film thickness, increasing film coverage and a higher rate of surface diffusion associated with higher temperature deposition, leading to an increase in the crystallite size. In the case of all films examined by PXRD, peaks attributable to Co$_2$Si ([031] $2\theta = 45.27°$)[45] CoSi ([210] $2\theta = 45.67°$; [211] $2\theta = 50.32°$)[46] and CoSi$_2$ ([220] $2\theta = 47.91°$)[47] were absent from the spectra.
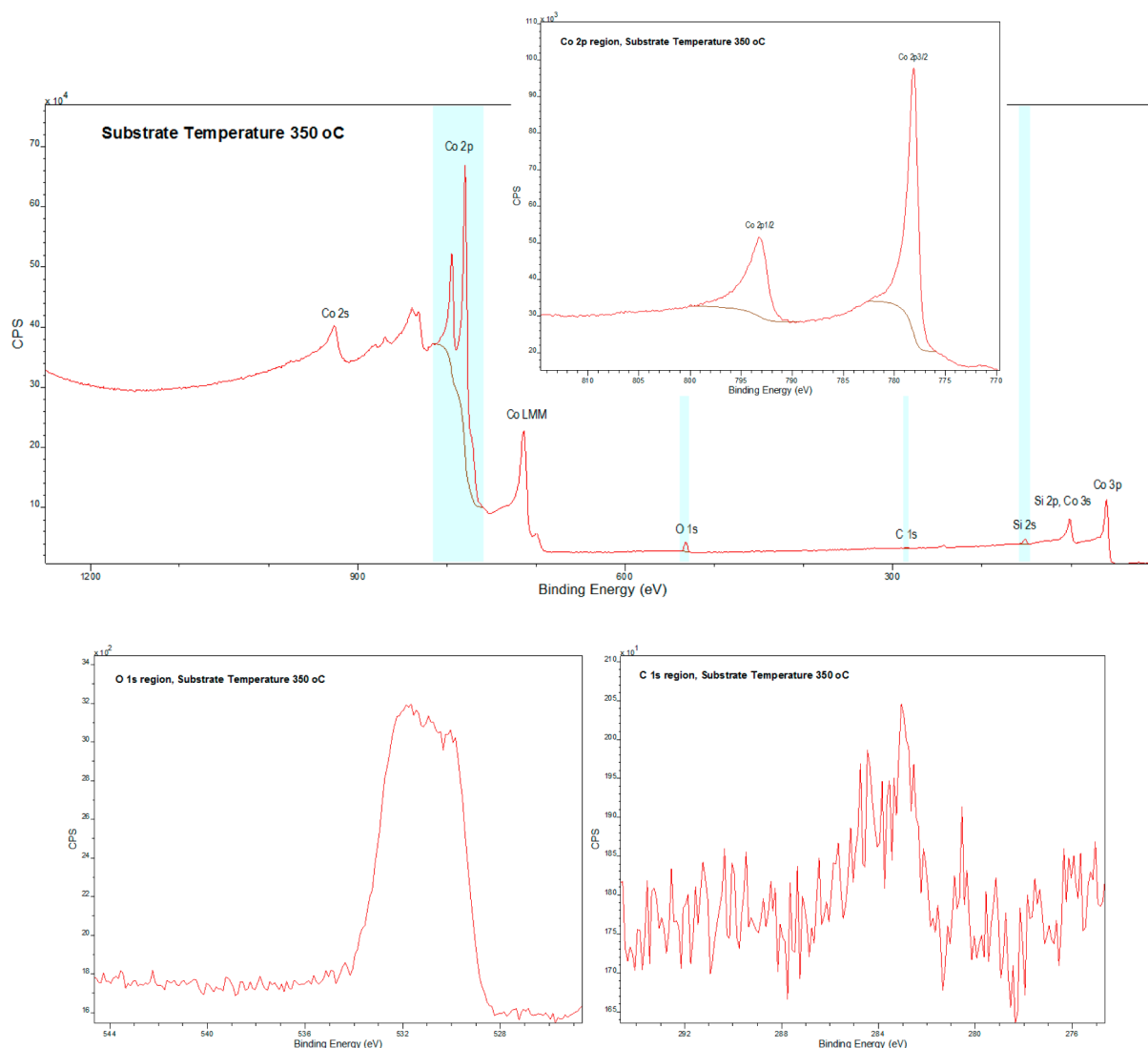
Figure 7. Survey XPS spectrum of a typical film deposited at a substrate temperature of 350 °C (above), with the Co2p region [793.24 eV (Co $2p_{1/2}$); 778.04 eV (Co $2p_{3/2}$)] highlighted (inset), and the 1s regions for oxygen (bottom left) and carbon (bottom right).

Table 7. Atomic % of Elements in Cobalt Thin Films Deposited at between 250 and 350 °C Post-Ar Etching (15 s)

substrate temperature	at.% Co	at.% O	at.% C	at.% Si
250 °C[a]	35.75	2.15	trace	62.10
275 °C[a]	11.10	1.53	trace	87.37
325 °C[a]	84.40	6.17	trace	9.43
350 °C[a]	80.13	7.52	1.08	11.27

[a]Quantification was performed assuming zero oxygen contribution from the silicon substrate. Values are expressed as atomic percentages.

Resistivity measurements were conducted using a four point probe on the two films deposited using complex **2a** at substrate temperatures of 325 and 350 °C (Table 8) which were shown by SEM analysis to be continuous; no measurements were conducted on samples deposited at lower deposition temperatures as the films were discontinuous. The average bulk resistivity values for films deposited at 350 and 325 °C were calculated to be 179.6 $\mu\Omega$ cm and 18.6 $\mu\Omega$ cm, the lower of which approaches the value for bulk cobalt (5.6 $\mu\Omega$ cm).[13e] The higher purity and continuity of films deposited at the lower
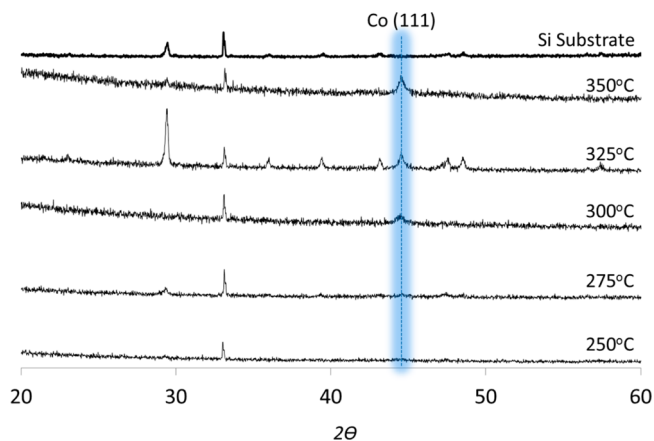
Figure 8. XRD patterns for an uncoated (400) silicon substrate and films deposited between 250 and 350 °C. Highlighted line shows the Co (111) Miller plane.

deposition temperature of 325 °C results in a lower resistivity value for the film, which is in agreement with previously reported data.[13m]

Table 8. Average Bulk Resistivity (ρ) and Sheet Resistance (R_S) Values for Continuous Cobalt Films Deposited at 325 and 350 °C Respectively Using Complex 2a[a]

temperature	thickness (nm) [growth rate (nm/min)]	R_S (Ω/□)	ρ ($\mu\Omega$ cm)
325	112 [3.73]	1.66	18.6
350	254 [8.47]	7.07	179.6

[a]The bulk resistivity of Cobalt = 5.6 $\mu\Omega$ cm (at 0 °C).

■ CONCLUSIONS

This paper reports the synthesis and thermal analysis of five CpCo(R$_2$-dab) complexes and reports the first study of their use as metal deposition precursors. Because of its high thermal stability and physical properties, compound **2a** was identified as a potential candidate for deposition studies. Thin films were deposited onto Si substrates in the temperature range of 250–350 °C under an atmospheric pressure of H$_2$. Films deposited at all temperatures were found to have low carbon contamination by XPS analysis, with varying degrees of oxygen incorporation, but only films deposited at a temperature ≥325 °C were continuous. The lowest measured resistivity was 18.6 $\mu\Omega$ cm for films deposited at 325 °C, which is in broad agreement with the purity and continuity of the films.

Films deposited at a substrate temperature of 300 °C and below were found to consist of a regular array of cobalt metal nanoclusters, the size of which appears to be dependent on the deposition temperature, and is likely to be dependent on the deposition time also. Those films which were crystalline, show that the deposited cobalt adopts the *fcc* crystal structure, as indicated by PXRD analysis; crystallinity and surface coverage were found to increase proportionally with increasing deposition temperature. More significantly, complex **2a** represents a precursor capable of depositing cobalt metal onto silicon substrates at a low enough temperature to preclude the concomitant formation of cobalt silicide.

Studies into the utility of complexes **2a–c** in ALD of cobalt thin films, at significantly lower temperatures are presently underway.

■ EXPERIMENTAL SECTION

Tristriphenylphosphine cobalt(I) chloride,[48] and sodium cyclopentadienide were all made according to literature procedures. *N,N*′-di-isopropyldiazabutadiene, *N,N*′-di-tertbutyldiazabutadiene, *N,N*′-dicyclohexyldiazabutadiene, *N,N*′-di-mesityldiazabutadiene, and *N,N*′-di-(2,6-di-isopropylphenyl)diazabutadiene were made using a modified general literature procedure.[49]

General Procedures. Elemental analyses were performed by Elemental Analysis Service, SASC, London Metropolitan University, London, U.K. ^{1}H and ^{13}C NMR spectra were recorded on a Bruker Avance 300 MHz FT–NMR spectrometer; chemical shifts are quoted in units of ppm, relative to Me$_4$Si (^{1}H, ^{13}C); coupling constants are in hertz (Hz).

All reactions were carried out under an inert atmosphere, and in the absence of light, using standard Schlenk techniques. Solvents were dried over activated alumina columns using an Innovative Technology solvent purification system (SPS) and degassed under an argon atmosphere. All other reagents were purchased from commercial sources.

Synthesis of 2a–e. 2a (η^5-C$_5$H$_5$)Co(η^2-^{i}Pr$_2$dab). A 2 M solution of sodium cyclopentadienyl in tetrahydrofuran (THF, 2.5 mL, 5 mmol) was added to a solution of tris(triphenylphosphine) cobalt(I) chloride (4.41 g, 5 mmol) in THF (30 mL) at −78 °C. The solution was allowed to warm to room temperature over a period of 1 h and was stirred for an additional hour. *N,N*′-Di-isopropyldiazabutadiene (0.70

g, 2 mmol) was then added, and the reaction mixture was refluxed for a period of 0.5 h, during which time a color change from deep red to brown was observed. The THF was removed in vacuo and the remaining material was extracted into hexane (3 × 20 mL); the combined extracts were filtered through Celite, the solvent was removed in vacuo, and the oily residue was distilled (5 × 10^{-2} mbar, 100 °C) yielding 0. 91 g (74%) of a yellow-brown liquid. Analysis. Calc.: C 59.09%, H 8.01%, N 10.60%; Found: C 58.93%, H 7.89%, N 10.54%. ^{1}H NMR (300.22 MHz, C$_6$D$_6$, 298 K) δ: 1.49 (d, 12H, ^{i}Pr-Me, *J* = 6.67 Hz), 4.56 (s, 5H, η^5-Cp), 4.93 (sep, 2H, ^{i}Pr-CH, *J* = 6.67 Hz), 6.96 (s, 2H, H<u>C</u>=N). ^{13}C{^{1}H} NMR (75.50 MHz, C$_6$D$_6$, 298 K) δ: 24.6 (^{i}Pr-<u>Me</u>), 64.2 (^{i}Pr-<u>CH</u>), 75.8 (η^5-Cp), 133.8 (H<u>C</u>=N).

Complexes **2b–e** were synthesized in an analogous manner to that of system **2a** with the exception of the addition of *N,N*′-di-tert-butyldiazabutadiene, **1b**, (0.84 g, 5 mmol) *N,N*′-dicyclohexylbutyl-diazabutadiene, **1c**, (1.10 g, 5 mmol), *N,N*′-dimesityldiazabutadiene, **1d**, (1.46g, 5 mmol), and *N,N*′-2,6-di-isopropylphenyldiazabutadiene, **1e**, (1.88 g, 5 mmol) respectively.

2b (η^5-C$_5$H$_5$)Co(η^2-^{t}Bu$_2$dab). Sublimation (5 × 10^{-2} mbar, 70 °C) yielded 1.13 g (77%) of a yellow-brown solid. Analysis. Calc.: C 61.63%, H 8.62%, N 9.58%; Found: C 61.54%, H 8.54%, N 9.46%. ^{1}H NMR (300.22 MHz, C$_6$D$_6$, 298 K) δ: 1.78 (s, 18H, ^{t}Bu), 4.73 (s, 5H, η^5-Cp), 7.17 (s, 2H, H<u>C</u>=N). ^{13}C{^{1}H} NMR (75.50 MHz, C$_6$D$_6$, 298K) δ: 32.8 (C<u>Me</u>$_3$), 64.9 (<u>C</u>Me$_3$), 75.7 (η^5-Cp), 134.9 (H<u>C</u>=N).

2c (η^5-C$_5$H$_5$)Co(η^2-Cy$_2$dab). Sublimation (5 × 10^{-2} mbar, 90 °C) yielded 1.05 g (61%) of a yellow-brown solid. Analysis. Calc.: C 66.25%, H 8.49%, N 8.13%; Found: C 66.16%, H 8.46%, N 8.12%. ^{1}H NMR (300.22 MHz, C$_6$D$_6$, 298 K) δ: 1.02−1.22 (m, 4H, C<u>H</u>$_2$), 1.32−1.51 (m, 4H, C<u>H</u>$_2$), 1.56−1.79 (m, 8H, C<u>H</u>$_2$), 2.39−2.52 (m, 4H, C<u>H</u>$_2$), 4.63 (s, 5H, η^5-Cp), 7.01 (s, 2H, H<u>C</u>=N). ^{13}C{^{1}H} NMR (75.50 MHz, C$_6$D$_6$, 298 K) δ: 25.1 (<u>C</u>H$_2$), 27.0 (CH$_2$), 36.0 (CH$_2$), 73.8 (<u>C</u>H), 76.0 (η^5-Cp), 134.4 (H<u>C</u>=N).

2d (η^5-C$_5$H$_5$)Co(η^2-Mes$_2$dab). Recrystallization from a saturated hexane solution at −28 °C yielded 1.17 g (56%) of a dark brown solid. Analysis. Calc.: C 72.10%, H 7.02%, N 6.72%; Found: C 72.21%, H 6.93%, N 6.66%. ^{1}H NMR (300.22 MHz, C$_6$D$_6$, 298 K) δ: 2.31 (s, 6H, *p*-<u>Me</u>), 2.41 (s, 12H, *o*-<u>Me</u>), 4.10 (s, 5H, η^5-Cp), 6.64 (s, 2H, H<u>C</u>=N,), 6.96 (s, 4H, Mes-C<u>H</u>). ^{13}C{^{1}H} NMR (75.50 MHz, C$_6$D$_6$, 298 K) δ: 18.6 (*o*-<u>Me</u>), 21.6 (*p*-<u>Me</u>), 77.0 (η^5-Cp), 129.1 (Mes-C<u>H</u>), 130.3 (*o*-<u>C</u>-Me), 134.6 (*p*-<u>C</u>-Me), 138.5 (H<u>C</u>=N), 157.2 (N-<u>C</u>).

2e (η^5-C$_5$H$_5$)Co(η^2-Dipp$_2$dab). Recrystallization from a saturated hexane solution at −28 °C yielded 1.43 g (57%) of a dark brown solid. Analysis. Calc.: C 74.38%, H 8.26%, N 5.57%; Found: C 74.28%, H 8.24%, N 5.57%. ^{1}H NMR (300.22 MHz, C$_6$D$_6$, 298 K) δ: 1.09 (d, 12H, ^{i}Pr-<u>Me</u>, *J* = 6.9 Hz), 1.43 (d, 12H, ^{i}Pr-<u>Me</u>, *J* = 6.9 Hz), 3.75 (sep, 4H, ^{i}Pr−C<u>H</u>, *J* = 6.9 Hz), 4.26 (s, 5H, η^5-Cp), 6.79 (s, 2H, H<u>C</u>=N), 7.22−7.26 (m, 4H, aryl-C<u>H</u>,), 7.31−7.38 (m, 2H, aryl-C<u>H</u>,). ^{13}C{^{1}H} NMR (75.50 MHz, C$_6$D$_6$, 298 K) δ: 23.7 (^{i}Pr-<u>Me</u>), 26.7 (^{i}Pr-<u>Me</u>), 28.7 (^{i}Pr-<u>CH</u>), 76.8 (η^5-Cp), 123.5 (*m*-<u>CH</u>), 126.9 (*p*-<u>CH</u>), 139.6 (H<u>C</u>=N), 141.6 (*o*-<u>C</u>), 156.5 (<u>C</u>-N).

Materials Chemistry. TGA Analysis of the complexes was performed at SAFC Hitech, Bromborough, U.K., using a Shimadzu TGA-51 Thermogravimetric Analyzer. Data points were collected every second at a ramp rate of 20 °C min^{-1} in a flowing (50 mL min^{-1}) N$_2$ stream. Thin films were deposited using a modified cold-walled CVD system (Electrogas Systems Ltd., U.K.). The system consisted of a tubular quartz reactor containing a silicon carbide coated graphite susceptor. The temperature of the susceptor was monitored using a k-type thermocouple coupled with a proportional−integral−derivative controller (PID controller), and heated with a water cooled IR lamp mounted externally beneath the reaction tube. The pressure of the system was maintained at 760 Torr throughout the deposition run, with the reactor lines and precursor, held in a bubbler, at 130 °C. The vapor generated was delivered to the reaction zone using a high purity hydrogen (99.998%) carrier gas (300 mL/min) metered from a mass flow controller. Films were deposited onto CVD coated ruthenium on silicon wafers at a susceptor temperature of between 250 and 300 °C. The total deposition time was 30 min.

Raman spectroscopy was recorded on a Renishaw InVia Raman using a 532 nm (green) laser. XPS measurements were performed on a

I

dx.doi.org/10.1021/ic402317g | *Inorg. Chem.* XXXX, XXX, XXX−XXX

Kratos Axis Ultra-DLD photoelectron spectrometer, utilizing monochromatic Al K$_\alpha$ radiation (photon energy 1486.6 eV), at the University of Cardiff. The instrument was precalibrated using pure gold and copper samples. Samples were sputtered for a predetermined set time over a 4 mm wide area using 4 kV argon ions using a minibeam I ion source. Spectra were collected at pass energies of 80 and 160 eV for high resolution and survey scans respectively, with the 100 μm aperture in place to focus on the center of the etch pit. FE-SEM analysis of the films was undertaken on a JEOL JSM-6480LV scanning electron microscope with EDX capability. TEM analysis was undertaken on a JEOL 1200EX, using nickel grids, at the University of Bath. AFM analysis was performed using a Digital Instruments Nanoscope IIIa, with TAP300 tips in contact mode (Tip radius <10 nm). Powder XRD of the films was performed on a Bruker D8 Powder Diffractometer, using a Cu anode X-ray source, (Kα wavelength = 1.5406 Å) at the University of Bath. Sheet resistivity measurements were recorded using a Jandel Multiheight 4-point probe in combination with a Guardian Surface Resistivity Meter Model #SRM-232-100, with a sheet resistance range of 0−100 ohm/sq.

Crystallography. Experimental details relating to the single-crystal X-ray crystallographic studies are summarized in Table 2. For both structures, data were collected on a Nonius Kappa CCD diffractometer at 150(2) K using Mo−Kα radiation (λ = 0.71073 Å). Structure solution and refinements were performed using SHELX86[50] and SHELX97[51] software, respectively. Corrections for absorption were made in all cases. Data were processed using the Nonius Software.[52] Structure solution, followed by full-matrix least-squares refinement was performed using the WINGX-1.80 suite of programs throughout.[53] For all complexes, hydrogen atoms were included at calculated positions. Data for complexes **2c** and **2d** are deposited with the Cambridge Structural Database with CCDC reference numbers 956829−956830.

■ ASSOCIATED CONTENT

Ⓢ Supporting Information
XPS spectra of the films deposited at 250 °C, 275 °C, 300 °C, 325 °C, and 350 °C are provided. X-ray crystallographic files in CIF format. This material is available free of charge via the Internet at http://pubs.acs.org.

■ AUTHOR INFORMATION

Corresponding Author
*E-mail: A.L.Johnson@bath.ac.uk. Phone: 44 (0)1225 384467. Fax: 44 (0)1225 386231.

Notes
The authors declare no competing financial interest.

■ ACKNOWLEDGMENTS

■ REFERENCES

(1) Kodas, T. T., Hampden-Smith, M. J., Eds.; *The chemistry of metal CVD*; VCH: Weinheim, Germany, 1994.

(2) (a) Pratt, W. P.; Lee, S. F.; Holody, P.; Yang, Q.; Loloee, R.; Bass, J.; Schroeder, P. A. *J. Magn., Magn. Mater.* **1993**, *126*, 406. (b) Pratt, W. P.; Lee, S. F.; Yang, Q.; Holody, P.; Loloee, R.; Schroeder, P. A.; Bass, J. *J. Appl. Phys.* **1993**, *73*, 5326.

(3) (a) Balke, B.; Wurmehl, S.; Fecher, G. H.; Felser, C.; Kubler, J. *Sci. Technol. Adv. Mater.* **2008**, 9. (b) Ernult, F.; Yakushiji, K.; Mitani, S.; Takanashi, K. *J. Phys.: Condens. Matter* **2007**, *19*. (c) Tsymbal, E. Y.; Belashchenko, K. D.; Velev, J. P.; Jaswal, S. S.; van Schilfgaarde, M.; Oleynik, I. I.; Stewart, D. A. *Prog. Mater. Sci.* **2007**, *52*, 401. (d) Yakushiji, K.; Mitani, S.; Ernult, F.; Takanashi, K.; Fujimori, H. *Phys. Rep.* **2007**, *451*, 1.

(4) Gay, J. G.; Richter, R. In *Ultrathin Magnetic Structures*; Bland, J. A. C., Heinrich, B., Eds.; Springer: Berlin, Germany, 1994; p 21.

(5) Lee, H.-B.-R.; Kim, H. *J. Cryst. Growth* **2010**, *312*, 2215.

(6) (a) Londergan, A. R.; Nuesca, G.; Goldberg, C.; Peterson, G.; Kaloyeros, A. E.; Arkles, B.; Sullivan, J. J. *J. Electrochem. Soc.* **2001**, *148*, C21. (b) Kutschera, M.; Groth, T.; Kentsch, C.; Shumay, I. L.; Weinelt, M.; Fauster, T. *J. Phys.: Condens. Matter* **2009**, 21. (c) Gross, M. E.; Kranz, K. S.; Brasen, D.; Luftman, H. *J. Vac. Sci. Technol. B* **1988**, *6*, 1548. (d) Rhee, H. S.; Ahn, B. T.; Sohn, D. K. *J. Appl. Phys.* **1999**, *86*, 3452. (e) Rhee, H. S.; Ahn, B. T. *J. Electrochem. Soc.* **1999**, *146*, 2720. (f) Rhee, H. S.; Ahn, B. T. *Appl. Phys. Lett.* **1999**, *74*, 3176. (g) Rhee, H. S.; Jang, T. W.; Ahn, B. T. *Appl. Phys. Lett.* **1999**, *74*, 1003. (h) Rhee, H. S.; Sohn, D. K.; Ahn, B. T. *Mater. Res. Soc., Symp. Proc.* **1999**, *564*, 145.

(7) (a) Henderson, L. B.; Ekerdt, J. G. *Microelectron. Eng.* **2010**, *87*, 588. (b) Khan, R. A.; Bhatti, A. S. *J. Magn. Magn. Mater.* **2010**, *323*, 340. (c) Olivier, S.; Decorps, T.; Calvo-Munoz, M.-L.; Da Silva, S.; Cayron, C.; Haumesser, P.-H.; Passemard, G. *Thin Solid Films* **2010**, *518*, 4773. (d) Zhang, L.; Ho, P. S.; Aubel, O.; Hennesthal, C.; Zschech, E. *J. Mater. Res.* **2011**, *26*, 2757. (e) Yang, C. C.; Flaitz, P.; Li, B.; Chen, F.; Christiansen, C.; Lee, S. Y.; Ma, P.; Edelstein, D. *Microelectron. Eng.* **2012**, *92*, 79. (f) Yang, C. C.; Baumann, F.; Wang, P. C.; Lee, S. Y.; Ma, P.; AuBuchon, J.; Edelstein, D. *Microelectron. Eng.* **2013**, *106*, 214.

(8) Cobo, S.; Heidkamp, J.; Jacques, P. A.; Fize, J.; Fourmond, V.; Guetaz, L.; Jousselme, B.; Ivanova, V.; Dau, H.; Palacin, S.; Fontecave, M.; Artero, V. *Nat. Mater.* **2012**, *11*, 802.

(9) (a) Ohzuku, T.; Ueda, A. *Solid State Ionics* **1994**, *69*, 201. (b) Ritchie, A. G. *J. Power Sources* **2004**, *136*, 285. (c) Wu, H. B.; Chen, J. S.; Hng, H. H.; Lou, X. W. *Nanoscale* **2012**, *4*, 2526. (d) Woo, J. H.; Trevey, J. E.; Cavanagh, A. S.; Choi, Y. S.; Kim, S. C.; George, S. M.; Oh, K. H.; Lee, S.-H. *J. Electrochem. Soc.* **2012**, *159*, A1120. (e) Scott, I. D.; Jung, Y. S.; Cavanagh, A. S.; Yan, Y.; Dillon, A. C.; George, S. M.; Lee, S.-H. *Nano Lett.* **2011**, *11*, 414. (f) Jung, Y. S.; Cavanagh, A. S.; Gedvilas, L.; Widjonarko, N. E.; Scott, I. D.; Lee, S.-H.; Kim, G.-H.; George, S. M.; Dillon, A. C. *Adv. Energy Mater.* **2012**, *2*, 1022. (g) Donders, M. E.; Arnoldbik, W. M.; Knoops, H. C. M.; Kessels, W. M. M.; Notten, P. H. L. *J. Electrochem. Soc.* **2013**, *160*, A3066.

(10) (a) Thurn-Albrecht, T.; Schotter, J.; Kastle, C. A.; Emley, N.; Shibauchi, T.; Krusin-Elbaum, L.; Guarini, K.; Black, C. T.; Tuominen, M. T.; Russell, T. P. *Science* **2000**, *290*, 2126. (b) Sellmyer, D. J.; Zheng, M.; Skomski, R. *J. Phys.: Condens. Matter* **2001**, *13*, R433. (c) Zhang, J.; Lima, F. H. B.; Shao, M. H.; Sasaki, K.; Wang, J. X.; Hanson, J.; Adzic, R. R. *J. Phys. Chem. B* **2005**, *109*, 22701.

(11) (a) Cheng, J. Y.; Ross, C. A.; Chan, V. Z. H.; Thomas, E. L.; Lammertink, R. G. H.; Vancso, G. J. *Adv. Mater.* **2001**, *13*, 1174. (b) New, R. M. H.; Pease, R. F. W.; White, R. L. *J. Vac. Sci. Technol., B* **1994**, *12*, 3196. (c) Ko, Y. K.; Park, D. S.; Seo, B. S.; Yang, H. J.; Shin, H. J.; Kim, J. Y.; Lee, J. H.; Lee, W. H.; Reucroft, P. J.; Lee, J. G. *Mater. Chem. Phys.* **2003**, *80*, 560.

(12) (a) Alameda, J. M.; Carmona, F.; Salas, F. H.; AlvarezPrado, L. M.; Morales, R.; Perez, G. T. *J. Magn. Magn. Mater.* **1996**, *154*, 249. (b) Sarkar, A.; Adhikari, R.; Das, A. K. *Phys. B* **2012**, *407*, 4148.

(13) (a) Boyd, E. P.; Ketchum, D. R.; Deng, H.; Shore, S. G. *Chem. Mater.* **1997**, *9*, 1154. (b) Charles, R. G.; Haverlac, Pg *J. Inorg. Nucl. Chem.* **1969**, *31*, 995. (c) Chioncel, M. F.; Haycock, P. W. *Chem. Vap. Deposition* **2005**, *11*, 235. (d) Dormans, G. J. M.; Meekes, G. J. B. M.; Staring, E. G. J. *J. Cryst. Growth* **1991**, *114*, 364. (e) Lane, P. A.; Oliver, P. E.; Wright, P. J.; Reeves, C. L.; Pitt, A. D.; Cockayne, B. *Chem. Vap. Deposition* **1998**, *4*, 183. (f) Lee, J.; Lee, J. G. *J. Korean Phys. Soc.* **2006**, *49*, S697. (g) Lee, J.; Park, H.; Lee, J. *Diffus. Defect Data, Pt. B* **2007**, *124−126*, 531. (h) Lee, K.; Park, T.; Lee, J.; Kim, J.; Kim, J.; Kwak, N.; Yeom, S.; Jeon, H. *Jpn. J. Appl. Phys.* **2008**, *47*, 5396. (i) Maruyama, T. *Jpn. J. Appl. Phys.* **1997**, *36*, L705. (j) Mordi, C. U.; Eleruja, M. A.; Taleatu, B. A.; Egharevba, G. O.; Adedeji, A. V.; Akinwunmi, O. O.; Olofinjana, B.; Jeynes, C.; Ajayi, E. O. B. *J. Mater. Sci. Technol.* **2009**, *25*, 85. (k) Papadopoulos, N.; Karayianni, C.-S.; Tsakiridis, P.; Sarantopoulou, E.; Hristoforou, E. *Chem. Vap. Deposition* **2011**, *17*,

J

dx.doi.org/10.1021/ic402317g | *Inorg. Chem.* XXXX, XXX, XXX−XXX

211. (l) Papadopoulos, N. D.; Illekova, E.; Karayanni, H. S.; Hristoforou, E. *J. Optoelectron. Adv. Mater.* **2008**, *10*, 1098. (m) Ye, D. X.; Pimanpang, S.; Jezewski, C.; Tang, F.; Senkevich, J. J.; Wang, G. C.; Lu, T. M. *Thin Solid Films* **2005**, *485*, 95.

(14) Ivanova, A. R.; Nuesca, G.; Chen, X. M.; Goldberg, C.; Kaloyeros, A. E.; Arkles, B.; Sullivan, J. J. *J. Electrochem. Soc.* **1999**, *146*, 2139.

(15) West, G. A.; Beeson, K. W. *Appl. Phys. Lett.* **1988**, *53*, 740.

(16) Choi, H.; Park, S. *Chem. Mater.* **2003**, *15*, 3121.

(17) Bandoli, G.; Barreca, D.; Gasparotto, A.; Maccato, C.; Seraglia, R.; Tondello, E.; Devi, A.; Fischer, R. A.; Winter, M. *Inorg. Chem.* **2009**, *48*, 82.

(18) Odedra, R.; Boag, N.; Anthis, J.; Kanjolia, R.; (Sigma-Aldrich Co., U.S.A.). Patent Application: WO 2011017068, 2011.

(19) Kim, K.; Lee, K.; Han, S.; Jeong, W.; Jeon, H. *J. Electrochem. Soc.* **2007**, *154*, H177.

(20) Lee, H.-B.-R.; Kim, H. *Electrochem. Solid State Lett.* **2006**, *9*, G323.

(21) (a) Lee, H.-B.-R.; Park, Y. J.; Baik, S.; Kim, H. *Chem. Vap. Deposition* **2012**, *18*, 41. (b) Diskus, M.; Nilsen, O.; Fjellvag, H. *Chem. Vap. Deposition* **2011**, *17*, 135. (c) Lee, H.-B.-R.; Kim, H. *Electrochem. Solid State Trans.* **2008**, *16*, 219.

(22) Kwon, J.; Saly, M.; Halls, M. D.; Kanjolia, R. K.; Chabal, Y. J. *Chem. Mater.* **2012**, *24*, 1025.

(23) (a) Li, Z.; Lee, D. K.; Coulter, M.; Rodriguez, L. N. J.; Gordon, R. G. *Dalton Trans.* **2008**, 2592. (b) Lim, B. S.; Rahtu, A.; Park, J.-S.; Gordon, R. G. *Inorg. Chem.* **2003**, *42*, 7951. (c) Wu, J.; Li, J.; Zhou, C.; Lei, X.; Gaffney, T.; Norman, J. A. T.; Li, Z.; Gordon, R.; Cheng, H. *Organometallics* **2007**, *26*, 2803. (d) Lim Booyong, S.; Rahtu, A.; Gordon Roy, G. *Nat. Mater.* **2003**, *2*, 749. (e) Kim, H. *Microelectron. Eng.* **2013**, *106*, 69.

(24) Knisley, T. J.; Saly, M. J.; Heeg, M. J.; Roberts, J. L.; Winter, C. H. *Organometallics* **2011**, *30*, 5010.

(25) (a) Donders, M. E.; Knoops, H. C. M.; van, M. C. M.; Kessels, W. M. M.; Notten, P. H. L. *J. Electrochem. Soc.* **2011**, *158*, G92. (b) Han, B.; Choi, K. H.; Park, J. M.; Park, J. W.; Jung, J.; Lee, W.-J. *J. Vac. Sci. Technol. A* **2013**, *31*, 01A145/1. (c) Klepper, K. B.; Nilsen, O.; Fjellvag, H. *J. Cryst. Growth* **2007**, *307*, 457. (d) Klepper, K. B.; Nilsen, O.; Fjellvag, H. *Thin Solid Films* **2007**, *515*, 7772.

(26) Dieck, H. T.; Haarich, M. *J. Organomet. Chem.* **1985**, *291*, 71.

(27) Sgro, M. J.; Stephan, D. W. *Dalton Trans.* **2010**, *39*, 5786.

(28) (a) Adams, R. D. *J. Am. Chem. Soc.* **1980**, *102*, 7476. (b) Zoet, R.; Vankoten, G.; Stufkens, D. J.; Vrieze, K.; Stam, C. H. *Organometallics* **1988**, *7*, 2118. (c) Zoet, R.; Jastrzebski, J. T. B. H.; Vankoten, G.; Mahabiersing, T.; Vrieze, K.; Heijdenrijk, D.; Stam, C. H. *Organometallics* **1988**, *7*, 2108. (d) Zoet, R.; Vankoten, G.; Muller, F.; Vrieze, K.; Vanwijnkoop, M.; Goubitz, K.; Vanhalen, C. J. G.; Stam, C. H. *Inorg. Chim. Acta* **1988**, *149*, 193. (e) Staal, L. H.; Vankoten, G.; Vrieze, K.; Vansanten, B.; Stam, C. H. *Inorg. Chem.* **1981**, *20*, 3598. (f) Staal, L. H.; Keijsper, J.; Polm, L. H.; Vrieze, K. *J. Organomet. Chem.* **1981**, *204*, 101. (g) Staal, L. H.; Vankoten, G.; Vrieze, K.; Ploeger, F.; Stam, C. H. *Inorg. Chem.* **1981**, *20*, 1830. (h) Staal, L. H.; Vankoten, G.; Vrieze, K. *J. Organomet. Chem.* **1981**, *206*, 99. (i) Staal, L. H.; Keijsper, J.; Vankoten, G.; Vrieze, K.; Cras, J. A.; Bosman, W. P. *Inorg. Chem.* **1981**, *20*, 555.

(29) Greulich, S.; Kaim, W.; Strange, A. F.; Stoll, H.; Fiedler, J.; Zalis, S. *Inorg. Chem.* **1996**, *35*, 3998.

(30) (a) Overbosch, P.; Vankoten, G.; Overbeek, O. *Inorg. Chem.* **1982**, *21*, 2373. (b) Overbosch, P.; Vankoten, G.; Spek, A. L.; Roelofsen, G.; Duisenberg, A. J. M. *Inorg. Chem.* **1982**, *21*, 3908.

(31) Lenges, C. P.; White, P. S.; Marshall, W. J.; Brookhart, M. *Organometallics* **2000**, *19*, 1247.

(32) Ni, C. B.; Stich, T. A.; Long, G. J.; Power, P. P. *Chem. Commun.* **2010**, *46*, 4466.

(33) Barral, M. C.; Delgado, E.; Gutierrezpuebla, E.; Jimenezaparicio, R.; Monge, A.; Delpino, C.; Santos, A. *Inorg. Chim. Acta* **1983**, *74*, 101.

(34) Laine, T. V.; Klinga, M.; Maaninen, A.; Aitola, E.; Leskela, M. *Acta Chem. Scand.* **1999**, *53*, 968.

(35) Rosa, V.; Gonzalez, P. J.; Aviles, T.; Gomes, P. T.; Welter, R.; Rizzi, A. C.; Passeggi, M. C. G.; Brondino, C. D. *Eur. J. Inorg. Chem.* **2006**, 4761.

(36) Tanabiki, M.; Sunada, Y.; Nagashima, H. *Organometallics* **2007**, *26*, 6055.

(37) Rosa, V.; Carabineiro, S. A.; Aviles, T.; Gomes, P. T.; Welter, R.; Campos, J. M.; Ribeiro, M. R. *J. Organomet. Chem.* **2008**, *693*, 769.

(38) Khusniyarov, M. M.; Harms, K.; Burghaus, O.; Sundermeyer, J. *Eur. J. Inorg. Chem.* **2006**, 2985.

(39) Sieger, M.; Hubler, K.; Scheiring, T.; Sixt, T.; Zalis, S.; Kaim, W. *Z. Anorg. Allg. Chem.* **2002**, *628*, 2360.

(40) Pronin, I. I.; Valdaitsev, D. A.; Voronchikhin, A. S.; Gomoyunova, M. V.; Contri, S. F.; Benedetti, S.; Lukes, P.; Valeri, S. *Tech. Phys. Lett.* **2005**, *31*, 494.

(41) Paranjape, M. A.; Mane, A. U.; Raychaudhuri, A. K.; Shalini, K.; Shivashankar, S. A.; Chakravarty, B. R. *Thin Solid Films* **2002**, *413*, 8.

(42) (a) Aprilesi, G.; Mazzega, E.; Michelini, M.; Nava, F.; Queirolo, G.; Meda, L. *J. Appl. Phys.* **1986**, *60*, 310. (b) Gruyters, M. *Surf. Sci.* **2002**, *515*, 53. (c) Wiemer, C.; Tallarida, G.; Bonera, E.; Ricci, E.; Fanciulli, M.; Mastracchio, G. F.; Pavia, G.; Marangon, S. *Microelectron. Eng.* **2003**, *70*, 233. (d) Pan, J. S.; Liu, R. S.; Zhang, Z.; Poon, S. W.; Ong, W. J.; Tok, E. S. *Surf. Sci.* **2006**, *600*, 1308.

(43) Liu, F. M.; Ye, J. H.; Ren, B.; Yang, Z. L.; Liao, Y. Y.; See, A.; Chan, L.; Tian, Z. Q. *Thin Solid Films* **2005**, *471*, 257.

(44) Owen, E. A.; Jones, D. M. *Proc. Phys. Soc., London B* **1954**, *67*, 456.

(45) Geller, S. *Acta Crystallogr.* **1955**, *8*, 83.

(46) Cheng, F. X.; Jiang, C. H.; Wu, J. S. *Mater. Trans.* **2004**, *45*, 2471.

(47) Li, Y. J.; Seidel, P.; Machalett, F.; Linzen, S.; Schmidl, F. *J. Mater. Res.* **1997**, *12*, 2072.

(48) Wakatsuki, Y.; Yamazaki, H. *Inorg. Synth.* **1989**, *26*, 189.

(49) O'Reilly, R. K.; Shaver, M. P.; Gibson, V. C.; White, A. J. P. *Macromolecules* **2007**, *40*, 7441.

(50) Sheldrick, G. M. *SHELX-86, Computer Program for Crystal Structure Determination*; University of Göttingen: Göttingen, Germany, 1986.

(51) (a) Sheldrick, G. M. *SHELX-97, Computer Program for Crystal Structure Refinement*; Univerity of Göttingen: Göttingen, Germany, 1997; (b) Sheldrick, G. M. *Acta Crystallogr. Sect. A* **2008**, *64*, 112.

(52) Otwinowski, Z.; Minor, W. Processing of X-ray Diffraction Data Collected in Oscillation Mode. In *Methods in Enzymology*; Carter, C. W., Jr., Sweet, R. M., Eds.; Academic Press: New York, 1997; Vol. *276*, Macromolecular Crystallography, part A, pp 307−326.

(53) Farrugia, L. J. *J. Appl. Crystallogr.* **2012**, *45*, 849.

■ NOTE ADDED AFTER ASAP PUBLICATION

This paper was published on the Web on November 15, 2013, with minor text errors in the Abstract. The corrected version was reposted on November 19, 2013.